Chinese Chemical Letters 34 (2023) 107299

Contents lists available at ScienceDirect

Chinese Chemical Letters

journal homepage: www.elsevier.com/locate/cclet

Fe_2O_3-decorated boron/nitrogen-co-doped carbon nanosheets as an electrochemical sensing platform for ultrasensitive determination of paraquat in natural water

Meng Li[a,b], Xinzhong Wang[a,*], Yelin Zhu[c], Xiuxiu Jia[c], Shusheng Zhang[b,*], Huaisheng Wang[d], Yongtao Li[e], Guangzhi Hu[a,c,**]

[a] School of Electronic Communication Technology, Shenzhen Institute of Information Technology, Shenzhen 518172, China
[b] College of Chemistry, Zhengzhou University, Zhengzhou 450000, China
[c] Institute for Ecological Research and Pollution Control of Plateau Lakes, School of Ecology and Environmental Science, Yunnan University, Kunming 650504, China
[d] School of Materials Science and Engineering, Liaocheng University, Liaocheng 252000, China
[e] Joint Institute for Environmental Research and Education, College of resources and environment, South China Agricultural University, Guangzhou 510642, China

ARTICLE INFO

Article history:
Received 14 December 2021
Revised 23 January 2022
Accepted 4 March 2022
Available online 7 March 2022

Keywords:
Paraquat
Fe_2O_3–BCN
Electrochemical sensor
Contaminant detection

ABSTRACT

Boron/nitrogen-co-doped carbon (BCN) nanosheets decorated with Fe_2O_3 nanocrystals (Fe_2O_3–BCN) were cast on a glassy carbon electrode (GCE) and applied as an electrochemical sensor to effectively detect paraquat (PQ), a toxic herbicide, in aqueous environments. A linear experiment performed using square wave voltammetry (SWV) under optimized experimental conditions produced a decent linear relationship and a low detection limit (LOD) of 2.74 nmol/L (S/N = 3). Repeatability, reproducibility, stability, and interference experiments confirmed that the Fe_2O_3–BCN/GCE system exhibited decent electrochemical sensing performance for PQ molecules. Notably, the designed sensor showed high selectivity and a decent linear relationship with PQ concentration in natural water samples. To the best of our knowledge, this is the first study on the preparation of Fe_2O_3–BCN nanosheets for PQ detection. The proposed sensor can be employed as an effective alternative tool for distinguishing and processing PQ.

Paraquat (PQ) was discovered as a chemical indicator by Weidel and Rosso in 1882, and subsequently promoted as an herbicide by Jealott's Hill in the United Kingdom in 1995 because of its redox properties [1,2]. PQ is a fast-killing insecticide with extremely high toxicity to humans and animals. Several countries have established requirements to limit the paraquat content in water, which is generally 30–200 nmol/L [3,4]. Although the European Union has banned the use of PQ, people in more than 100 countries use PQ in agricultural production. Over the past decade, more than a thousand people have died of PQ poisoning [5]. Therefore, rapid detection of paraquat in aquatic environments with a low detection limit is indispensable.

PQ detection has been achieved using various methods such as high-performance liquid chromatography [6,7], gas chromatography-mass spectrometry [8], spectrophotometry [9], fluorescence [10], and capillary electrophoresis [11]. Although paraquat can be rapidly and selectively detected using these methods, disadvantages such as low recognition ability, complicated operation, and cumbersome equipment make them unsuitable for use as portable on-site detection equipment [10,12]. In this regard, electrochemical methods offer benefits such as low limits of detection (LODs) and rapid, mobile, and convenient analysis [13,14]. Moreover, electrochemical methods permit the use of square wave voltammetry (SWV), cyclic voltammetry (CV), and differential pulse voltammetry (DPV) for PQ analysis and measurement.

Nanocomposites are currently popular in scientific research and industry owing to their excellent performance in various applications [15–17]. Several nanocomposite-based electrochemical sensors, such as those based on Au nanoparticles and graphene (AuNPs/GAQ) [18] and Au nanocrosses and chitosan (AuNCs–CS) [19], have been developed over the last decade for PQ detec-

* Corresponding authors.
** Corresponding author at: School of Electronic Communication Technology, Shenzhen Institute of Information Technology, Shenzhen 518172, China
E-mail addresses: wangxz@sziit.com.cn (X. Wang), zsszz@126.com (S. Zhang), guangzhihu@ynu.edu.cn (G. Hu).

https://doi.org/10.1016/j.cclet.2022.03.022
1001-8417/

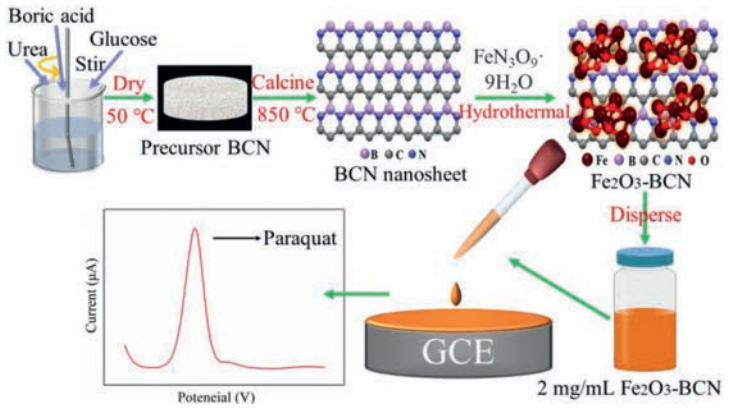

Fig. 1. Schematic of the synthesis of BCN and Fe_2O_3–BCN, and the experimental flowchart.

tion. Boron/nitrogen-co-doped carbon (BCN) is a non-metal semiconductor with adjustable bandwidth and a graphene-like two-dimensional non-metal layered material with excellent electrochemical performance [20–22]. The outstanding performance of BCN is due to its excellent thermal [23], optical [24], and mechanical properties [25], which have led to a surge in research involving the synthesis and characterization of novel, BCN-based materials globally. In fact, loading a certain amount of a metal on the BCN material can enhance its electrochemical performance [26–28]. Electrochemical sensors synthesized using BCN have exhibited excellent performance [29,30]. For example, Chen *et al.* [31] synthesized two-dimensional boron-nitride/carbon-nanotube nanosheets to detect lipocalin-2 in clinical serum specimens, and Li *et al.* [32] synthesized single-atom niobium-doped boron–carbon–nitrogen nanotubes (SANb–BCN) to detect nitrobenzene in an aqueous environment.

Fe_2O_3 has a wide range of sources and is the main component of hematite and rust. Therefore, nanosheets of BCN and Fe_2O_3–BCN were synthesized in this study *via* a hydrothermal reaction and high-temperature calcination for PQ detection. Fig. 1 illustrates the preparation of the investigated materials. Characterization techniques such as transmission electron microscopy (TEM), scanning electron microscopy (SEM), thermogravimetric analysis (TGA), and X-ray diffraction (XRD) were employed to determine the morphology of the Fe_2O_3–BCN nanosheets. Moreover, Fe_2O_3–BCN/glass-carbon-electrode (GCE), BCN/GCE, and Fe_2O_3/GCE were similarly prepared. Comparison of the electrochemical performance of the three modified electrodes and bare GCE revealed the superior electrochemical sensing performance of Fe_2O_3–BCN/GCE. The electrochemical behavior of PQ on the electrode was examined by changing the scan rate in CV. Subsequently, optimal current response conditions were determined by modifying and controlling the amount of Fe_2O_3–BCN coated on the electrode, the enrichment time, deposition potential, and electrolyte pH. Under the optimized conditions, Fe_2O_3–BCN/GCE showed decent linearity, a low LOD, and selection specificity for PQ. Finally, the modified electrodes were used to analyze the target pollutant in actual water samples (tap water and lake water), and the satisfactory recovery rate and linear relationship had been achieved.

Ultrapure water with a resistance of ≥18.25 MΩ/cm was used to prepare all the solutions used in this study. All the reagents were analytically pure and used directly without purification. Paraquat (≥99.7%) was purchased from Macklin (Shanghai, China). Urea (CH_4N_2O) (≥99%) and boric acid (H_3BO_3; ≥99.5%) were purchased from Rhawn (Shanghai, China). Ferric nitrate nonahydrate (≥98.5%) and glucose ($C_6H_{12}O_6$) (≥99%) were purchased from Macklin (Shanghai, China). PBS buffer composed of Na_2HPO_4 (Aladdin) (≥99%) and NaH_2PO_4 (Aladdin) (≥99%) was freshly prepared at a concentration of 0.1 mol/L. A CHI 660E electrochemical workstation (Shanghai Chenhua Instrument Co., Ltd., China) was used for electrochemical measurements at room temperature. Both the SWV and CV responses were acquired using a three-electrode system containing a working electrode (GCE, BCN/GCE, or Fe_2O_3–BCN/GCE), reference electrode (Ag/AgCl), and counter electrode (Pt).

Briefly, the BCN nanosheets were prepared as following: Urea (3 g), boric acid (3.09 g), and glucose (1.02 g) were stirred and dissolved in 20 mL of ultrapure water. The resulting mixture was dried in a vacuum drying oven at 50 °C for 12 h, which yielded a white powder. This product was calcined at 850 °C for 4 h within N_2 atmosphere to produce the BCN nanosheets. The BCN material (0.07 g) and ferric nitrate nonahydrate (1.13 g) were dissolved in 70 mL of water, and subjected to a hydrothermal reaction in a reaction kettle at 200 °C for 12 h. The resulting black solid material was washed repeatedly with ethanol. Finally, the black solid was dried in a blast drying box at 50 °C for 6 h to yield Fe_2O_3–BCN, similar to the protocol followed in our recent study [33].

The surface of the GCE was cleaned until it was smooth, and subsequently polished on a suede material using polishing powder with specifications of 1 μm and 100 nm. After each polishing step, deionized water, ethanol, and acetone were used to ultrasonically treat the polished GCE for 10 s. The surface of the treated GCE was dried thereafter under nitrogen for subsequent use. BCN (2 mg) and Fe_2O_3–BCN (2 mg) were added to two separate bottles, followed by the addition of ultrapure water (1 mL), and sonication of the mixtures for 30 min to ensure uniform dispersion. The two dispersions (10 μL) were dropped on two vertical GCE surfaces and subsequently air-dried at room temperature (20 °C) for 24 h to obtain BCN/GCE and Fe_2O_3–BCN/GCE.

A test range of 0−1 V was adopted for SWV and CV. Moreover, CV was performed at 50 mV/s, and SWV was conducted with a potential increment of 4 mV, amplitude of 25 mV, and frequency of 15 Hz. To remove the dissolved oxygen in the electrolyte solution requires bubbling with N_2 for 10 min. The SWV test required the use of *i-t* curves to deposit the investigated pollutants on the electrode surfaces. An applied voltage of −0.2 V and an enrichment time of 100 s were used to obtain the *i-t* curves. The electrolyte for the SWV and CV tests contained PBS (10 mL, 0.1 mol/L, pH 6.0) and 10 μmol/L PQ.

SEM analysis (Fig. 2a) indicated that the prepared BCN and Fe_2O_3–BCN materials were present in the form of nanosheets, and the surfaces of the BCN nanosheets were relatively smooth. Furthermore, TEM analysis (Fig. 2b) suggested that the Fe_2O_3–BCN nanosheets had a rough surface with a uniform, thick layer of Fe_2O_3 particles. Fig. 2c is the SEM image of Fe_2O_3–BCN after electrochemical measurement. The appearance of Fe_2O_3–BCN did not

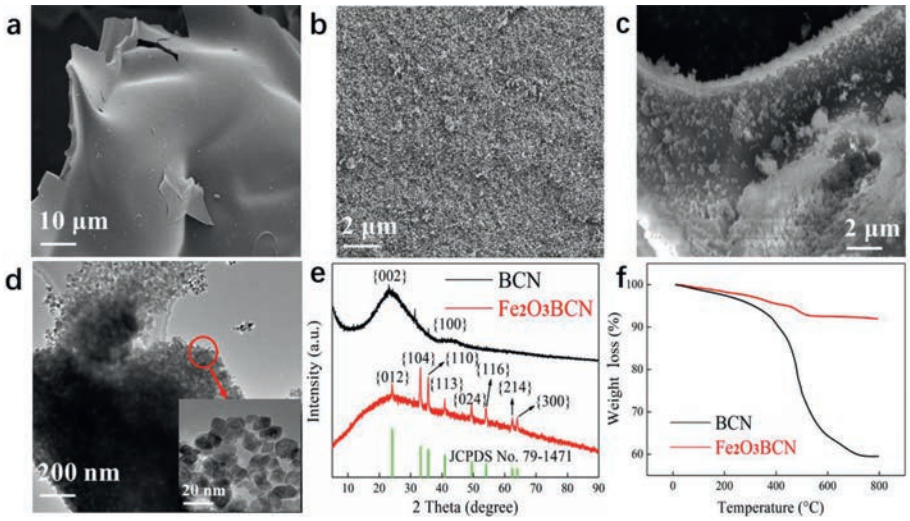

Fig. 2. SEM images of the (a) BCN and (b) Fe_2O_3–BCN materials. (c) SEM images of Fe_2O_3–BCN after electrochemical measurements. (d) TEM image of Fe_2O_3–BCN; the inset shows a high-magnification TEM image. (e) XRD patterns of BCN and Fe_2O_3–BCN. (f) Thermogravimetric analysis of BCN (black) and Fe_2O_3–BCN (red).

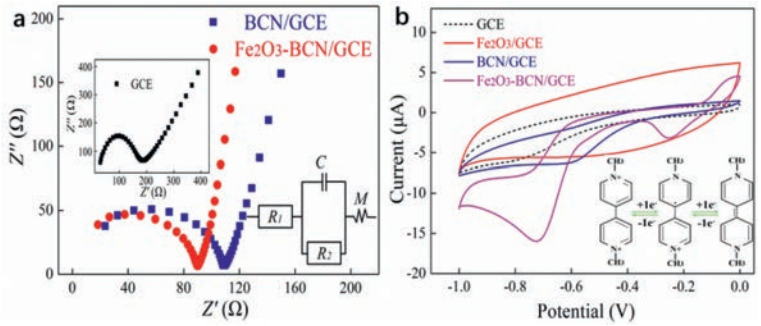

Fig. 3. (a) Nyquist plots of BCN/GGE (blue) and Fe_2O_3–BCN/GCE (red) collected using an electrolyte containing 5.0 mmol/L $K_3Fe(CN)_6$–$K_4Fe(CN)_6$ and 0.1 mol/L KCl. The inset shows the Nyquist diagram of the GCE, and another inset is simple equivalent circuit. (b) CV curves of GCE, Fe_2O_3/GCE, BCN/GCE, and Fe_2O_3–BCN/GCE obtained using an electrolyte containing 0.1 mol/L PBS and 1.0 μmol/L PQ (scan rate: 50 mV/s). The inset shows the reaction mechanism of paraquat.

change significantly after measurement. The XRD pattern of BCN shows broad and soft peaks at 24° and 43°, respectively, which were attributed to the (002) and (100) crystal planes, respectively [34]. The XRD pattern of Fe_2O_3–BCN (red profile in Fig. 2d) shows peaks at 24.149°, 33.158°, 35.631°, 40.862°, 49.462°, 54.069°, 62.436° and 64.000°, which were ascribed to the crystal planes of (012), (104), (110), (113), (024), (116), (214) and (300), respectively. Generally, the broad diffraction peaks on the XRD spectrum indicate that the synthesized material has poor crystallinity. In Fig. 2e, the broad peak of Fe_2O_3–BCN at 24° is narrower than that of BCN, indicating that the crystallinity of BCN is poor, which is consistent with the results shown by TEM and SEM. Moreover, careful comparison revealed that the XRD data of Fe_2O_3–BCN were consistent with those of hematite syn (JCPDS No. 79-1471).

Fig. 2f is thermogravimetric analysis of BCN and Fe_2O_3–BCN. The mass of BCN and Fe_2O_3–BCN were both 10 mg. The calcination conditions were nitrogen atmosphere, heating at 15 °C/min and stopping at 800 °C. Final BCN mass remaining 59.9 wt%, Fe_2O_3–BCN mass remaining 92.6 wt%. According to the calculation, the load of Fe_2O_3 is about 32.7 wt%. These results validate the successful synthesis of the Fe_2O_3–BCN nanosheets.

Electrochemical impedance analysis (EIS) of bare GCE, BCN/GCE, and Fe_2O_3–BCN/GCE was performed to assess the electrochemical sensing performance of Fe_2O_3–BCN/GCE. Fig. 3a shows the Nyquist plots of the three electrodes, which indicate that the charge-transfer resistance (R_{ct}) of Fe_2O_3–BCN/GCE is lower than those of BCN/GCE and GCE. In the equivalent circuit diagram of the illustration, R_1 represents the resistance of the electrolyte, and R_2 represents the R_{ct}. C and M represent the double-layer capacitance and mass transfer generated at the interface between electrode and electrolyte solution, respectively. The corresponding R_2 values of GCE, BCN/GCE and Fe_2O_3–BCN/GCE were 195, 112 and 88 Ω, respectively. The wider semicircles of BCN/GCE and GCE indicate their poor electron-transfer activity and electronic conductivity [35,36]. These results indicate the formation of an effective electron-conduction path between Fe_2O_3–BCN/GCE and the electrolyte [37], which confirms the optimal conductivity of the Fe_2O_3–BCN/GCE system. CV curves of Fe_2O_3–BCN/GCE, BCN/GCE, and GCE were collected using 0.1 mol/L PBS containing 1 μmol/L PQ. Generally, the Nyquist diagram appears as a straight line with a tilt angle of $\pi/4$ (45°) for diffusion-controlled reactions on electrode surfaces. Fig. 3a clearly shows that the reaction on the bare electrode surface is controlled by diffusion, whereas those on the modified electrodes are not.

Fig. 3b shows that the GCE and Fe_2O_3/GCE has almost no redox current in response to PQ, and BCN/GCE produces a weak current response to PQ at approximately −0.61 V. In contrast, the Fe_2O_3–BCN/GCE system exhibited a more robust current response at −0.25 V and −0.71 V. The inset in Fig. 3b shows the redox reactions of PQ. In a complete CV curve, PQ first obtains an electron to be reduced to an intermediate, and then obtains an electron to become a reduced state. Then it loses two consecutive electrons and is oxidized back to the original PQ. Fe_2O_3 particles have a huge specific surface, and the surface effect is obvious and has a

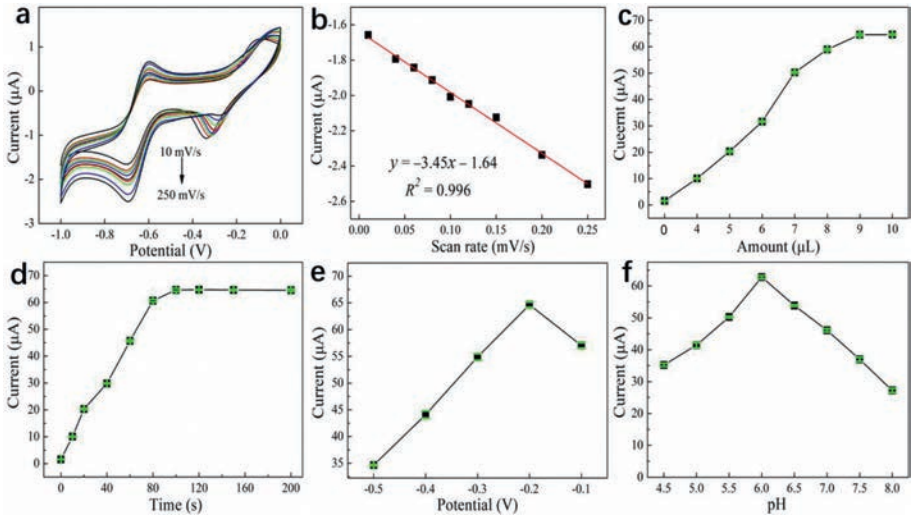

Fig. 4. (a) CV curves obtained at different scanning speeds in 0.1 mol/L PBS containing 1 μmol/L PQ in a scanning rate range of 10–250 mV/s. (b) Linear relationship between the scan rate and the current response. (c) Impact of the amount of Fe_2O_3–BCN on signal response. Effects of the (d) duration and (e) deposition potential on current. (f) Signal response in the pH range of 4.5–8.0 in 0.1 mol/L PBS containing 10 μmol/L PQ.

certain degree of oxidation [38]. Moreover, due to the small size of iron oxide particles, the volume percentage of the surface is large, the bond state and electronic state of the surface are different from those inside the particles, and the coordination of surface atoms is different, which leads to the increase of the active site of the surface. BCN is used to enhance conductivity, and the doping of B and N atoms can provide more sites. In the three-electrode system, each step of paraquat reaction needs to get or lose an electron, while Fe_2O_3–BCN has more active sites and certain oxidation. The red curve in Fig. 3b has two peaks at −0.25 V and −0.71 V, which are consistent with the two reductions of PQ. Fe_2O_3–BCN/GCE exhibits a stronger response to the CV current generated by PQ, which is more in line with the redox behavior of PQ [39]. These electrochemical test results reveal the suitability of Fe_2O_3–BCN/GCE as an electrochemical sensor for PQ detection.

The reaction mechanism of an analyte at electrode surfaces can be analyzed using CV curves obtained at different scanning rates [40]. The control process at electrode surfaces can occur *via* surface or diffusion control. As shown in Fig. 4a, the current response gradually increased with increasing scan rate, and a linear relationship was established between these parameters (Fig. 4b). Essentially, the scan rate was positively correlated with the current signal. This indicates that the reaction on the electrode surface was dominated by surface adsorption control [41].

A series of conditions was optimized to maximize the current signal of the Fe_2O_3–BCN/GCE sensor to PQ. The Fe_2O_3–BCN coating on the surface of the electrode affects the electronic conductivity, which consequently influences the current signal response [42]. Therefore, the influence of the amount of Fe_2O_3–BCN used to modify the GCE on current response was examined first. The current signal intensity rapidly increased with increasing amount of Fe_2O_3–BCN dropped on the electrode surface in the range of 0–7 μL, and reached a maximum at 9 μL (Fig. 4c). When the surface tension of a dispersion is constant, the amount of a material used for electrode modification within a specific range increase, which enhances the current response signal. The dispersion and eventual saturation of the added material on the electrode surface leads to stabilization of the current response.

The experimental procedure was optimized after the electrode optimization step. The current response clearly increased with increasing enrichment time, and stabilized after an enrichment time of 100 s (Fig. 4d). Additionally, five enrichment potentials of −0.1, −0.2, −0.3, −0.4, and −0.5 V were tested (Fig. 4e), which resulted in the current response achieving a maximum at a potential of −0.2 V. Because a further increase or decrease in voltage did not enhance the current, the oxidation reaction of PQ was presumed to proceed within a certain voltage range. Once the voltage exceeded a certain threshold, side reactions could occur, and the oxidation of PQ no longer dominated the electrolyte.

The reduction performance of Fe_2O_3–BCN for PQ was investigated in the pH range of 4.5–8.0 (Fig. 4f) to avoid the decomposition of PQ, which typically occurs under excessively alkaline conditions [43]. The current response increased and subsequently decreased with increasing pH, reaching a maximum at a pH of 6.0. The use of a slightly acidic electrolyte, which contains a small amount of H^+ ions, promotes the oxidation of PQ by Fe_2O_3–BCN/GCE in the electrolyte. However, the use of an excessively acidic electrolyte leads to the production of protons by the functional groups on the electrode surface owing to the numerous H^+ ions, which hinders the adsorption of PQ on the electrode surface [44]. Therefore, the electrochemical behavior of the electrode surface was clearly affected by pH, and an optimal pH of 6.0 was employed for PQ detection in the subsequent experiments.

SWV curves were obtained using 0.1 mol/L PBS buffer solutions containing different concentrations of PQ under the optimized conditions. The SWV curves and the corresponding linear relationships (Fig. 5) indicate that the current response gradually increased with increasing PQ concentration; moreover, these parameters were found to be linearly related. The linearity was divided into two concentration ranges: 10–800 nmol/L and 0.8–12 μmol/L. In an electrochemical test, the adsorption of the tested substrates onto the electrode surface induces a current response that can be detected. However, at extremely low PQ concentrations, the active sites on the sensor surface will not be saturated, resulting in a rapid increase in the current response. Moreover, when the reactant concentration is relatively high, the active sites on the sensor surface are occupied to a certain extent, leading to a decrease in the current response growth rate [45].

Therefore, the linear range was fitted piecewise in a conventional manner, which yielded a satisfactory linear relationship (R^2). The regression equations obtained by linear fitting are expressed as follows:

10–800 nmol/L: I (μA) = 8.898C (PQ/μmol/L) + 0.948, R^2 = 0.997,

0.8–12 μmol/L: I (μA) = 7.959C (PQ/μmol/L) + 41.11, R^2 = 0.999.

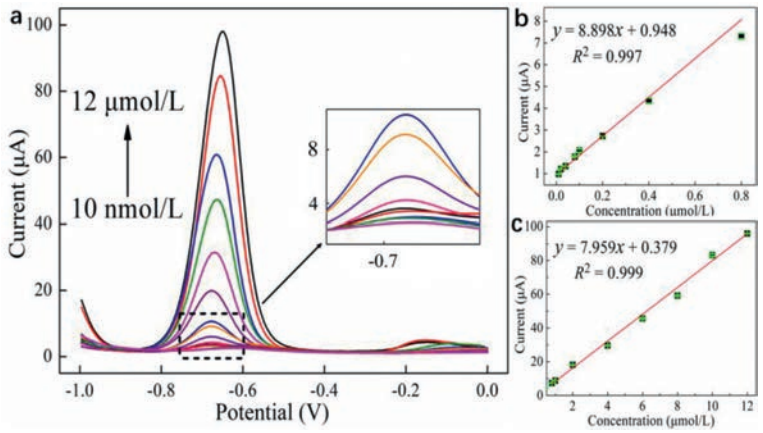

Fig. 5. (a) SWV curves obtained under the optimized conditions (pH 6.0, 0.1 mol/L PBS) in a PQ concentration range from 10 nmol/L to 12 μmol/L, and the inset was the enlarged image in the imaginary line. Linear relationships between the current response and PQ concentration in the ranges of (b) 10–800 nmol/L and (c) 0.8–12 μmol/L.

Table 1
Various modified electrodes used for electrochemical determination of PQ.

Modified electrode	Detection method	Linear range (μmol/L)	LOD (nmol/L)	R^2	Ref.
MSTF/GCE	SWV	0.5–10	12	0.946	[47]
SIPE/GCE	SWV	3.0–100	800	0.999	[48]
N/AgNP/MWCNT/GCE	DPV	0.1–10	68	0.996	[49]
BF/GCE	DPV	0.1–4.2	8.9	0.996	[50]
BN/MoS_2/AuNPs/GCE	DPV	0.1–100	74	0.994	[46]
AuNPs/GAQ/GCE	DPV	0.02–24	6	0.998	[18]
PPY–NGE/GCE	DPV	0.05–2	41	0.999	[51]
HAP–CPE	SWV	0.8–20	15	0.991	[52]
Fe_2O_3–BCN/GCE	SWV	0.01–0.8, 0.8–12	2.7	0.997, 0.999	This work

MSTF: mesoporous silica thin-films; SIPE: silver inkjet-printed electrodes; AgNP: Ag nanoparticles; MWCNT: multi-walled carbon nanotubes; BF: bismuth film; BN: boron nitride; AuNPs: Au nanoparticles; AuNPs/GAQ: Au nanoparticle/8-aminoquinoline-functionalized graphene oxide; PPY–NGE: polypyrrole nitrogen-doped; HAP–CPE: hydroxyapatite carbon paste electrode.

The LOD was calculated using the equation, LOD = 3Sb/*S* [46], where Sb is the standard deviation of the current signal detected by the blank solution 10 times, and *S* is the slope of the calibration curve. The LOD of Fe_2O_3–BCN/GCE to PQ was estimated to be 2.74 nmol/L (S/N = 3). Several typical materials that have been examined for the electrochemical detection of PQ and their corresponding parameters are listed in Table 1 [18,46-52]. The international minimum PQ emission standard is considerably greater than the LOD of the designed Fe_2O_3–BCN/GCE sensor [53]. Comparison of the performance data listed in Table 1 reveals the potential of Fe_2O_3–BCN/GCE as an excellent chemical sensor for PQ detection.

The SWV method was used to test the designed electrode against five identical solutions in the presence of 10 μmol/L PQ in a 0.1 mol/L PBS buffer solution to determine whether they contained similar amounts of PQ. The current responses of the electrode to the five solutions (Fig. 6a) had an error of less than 3%, indicating excellent repeatability. Additionally, the responses of five electrodes to a current signal using the same 0.1 mol/L PBS electrolyte containing 10 μmol/L PQ were almost identical (Fig. 6b). Moreover, the signal responses of the electrode on the first, seventh, and fifteenth days were almost similar (Fig. 6c). These results indicate the remarkable repeatability, reproducibility, and ultrastable characteristics of the Fe_2O_3–BCN/GCE sensor. The selectivity and anti-interference ability of Fe_2O_3–BCN/GCE were studied in the presence of different inorganic and organic substances (Fig. 6d). The a–j entries in the plot represent 100 × concentrations of Mg^{2+}, thiourea, urea, Zn^{2+}, K^+, Fe^{2+}, Ca^{2+}, Fe^{3+}, ascorbic acid, and benzalkoniumchloride compared to that of PQ. An interference of less than 3% was observed in the presence of the interfering substances. These results reveal the strong selectivity and anti-interference ability of Fe_2O_3–BCN/GCE.

The suitability of the Fe_2O_3–BCN/GCE electrochemical sensor for detecting PQ in actual water samples was examined, and the practicability and feasibility of the modified electrode were assessed. The standard addition method was employed with tap water and lake water to detect PQ in actual water samples. Because the tap water and lake water were clear, they were used directly without pretreatment. However, PQ was not detected in the tap water or lake water. The test results of the designed sensor on water samples are consistent with the results obtained by LC-MS. The LC is Nexera X2 from Shimadzu (Japan), and the MS is 6500 from ABSCIEX (American). Therefore, certain concentrations of PQ were sequentially added to the water samples to obtain a linear relationship. The test results for tap water (Fig. 6e) indicate decent linearity ($R^2 = 0.999$), with recovery rates of 99.8% and 99.4% for 0.6 μmol/L PQ and 1.5 μmol/L PQ, respectively. Moreover, the detection results for the lake water (Fig. 6f) indicate decent linearity ($R^2 = 0.999$), with recovery rates of 99.4% and 99.8% for 0.6 μmol/L PQ and 1.5 μmol/L PQ, respectively. These results led to a high linear correlation coefficient and an excellent recovery rate. The chemical sensing performance and detection in real water samples achieved by the designed sensor can lead to promising practical applications.

In summary, a simple and low-cost Fe_2O_3–BCN/GCE electrochemical sensor was prepared successfully. The different electrochemical responses of PQ obtained with bare GCE, BCN/GCE, Fe_2O_3/GCE and Fe_2O_3–BCN/GCE based electrochemical sensors confirmed that Fe_2O_3–BCN exhibited excellent electrochemical sensing performance for PQ. Under the optimized conditions, the developed electrochemical sensor exhibited a broad linear range, a low LOD, and high selectivity, repeatability, reproducibility, and stability. Additionally, the Fe_2O_3–BCN-based electrochemical sensor

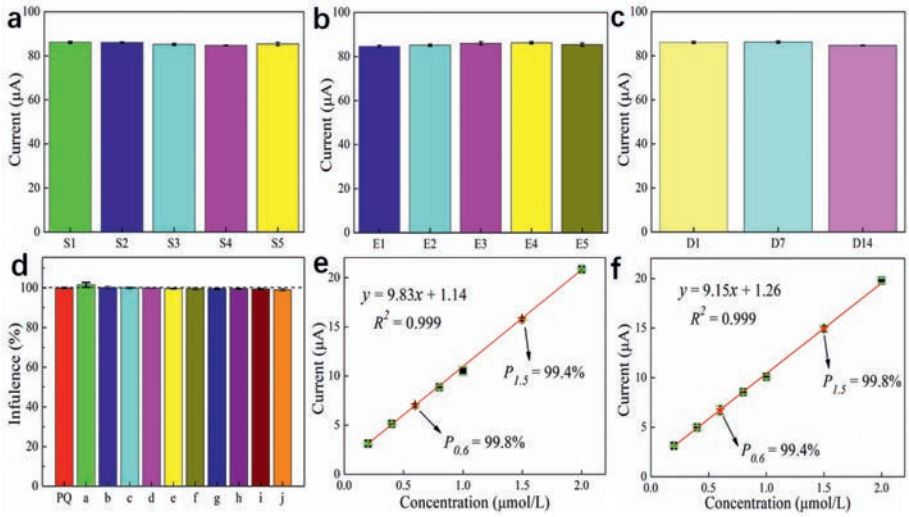

Fig. 6. (a) Signal responses obtained using five separate samples containing similar concentrations of PQ. (b) Current signal responses of five modified electrodes obtained using identical electrolytes. (c) Signal responses of a modified electrode on the first, seventh, and fourteenth days. (d) Interference analysis conducted using Mg^{2+}, thiourea, urea, Zn^{2+}, K^{+}, Fe^{2+}, Ca^{2+}, Fe^{3+}, ascorbic acid, and benzalkoniumchloride, corresponding to a–j, respectively. The interferent concentrations were all 100× higher than that of PQ. Detection of PQ using Fe_2O_3–BCN/GCE in (e) tap water and (f) water from Lake Yangzonghai. The red star represents the added standard sample.

was successfully applied to detect PQ in both lake and tap water samples with satisfactory results. Hopefully, the proposed sensor could be used as an effective alternative tool for distinguishing and processing PQ.

Declaration of competing interest

The authors declare that they have no known competing financial interests or personal relationships that could have appeared to influence the work reported in this paper.

Acknowledgments

This work was funded by the National Key Research and Development Program (No. 2019YFC1804400), the National Natural Science Foundation of China (Nos. 21974124, 22004109, 22076174), Guangdong Province Higher Vocational Colleges & Schools Pearl River Scholar Funded Scheme (2016), Guangdong Third Generation Semiconductor Engineering Technology Development Center (No. 2020GCZX007), the Yunnan Provincial Science and Technology Bureau and the Double Top Joint Fund of Yunnan University (No. 2019FY003025) and the Double First Class University Plan (No. C176220100042).

References

[1] H. Zhang, K.-T. Huang, L. Ding, et al., Chin. Chem. Lett. 30 (2021) 9–54.
[2] H.T. Xi, T.T. Yi, X.Q. Sun, Chin. Chem. Lett. 21 (2010) 633–636.
[3] J. Chen, Y. Su, F. Lin, et al., Ecotoxicol. Environ. Saf. 224 (2021) 112711.
[4] Q.Q. Li, Y.P. Du, Y. Xu, et al., Chin. Chem. Lett. 24 (2013) 332–334.
[5] T.M. Wijerathna, F. Mohamed, I.B. Gawarammana, et al., Ecotoxicol. Environ. Saf. 80 (2020) 103510.
[6] N. Halim, A. Kuntom, R. Shinde, K. Banerjee, Eur. J. Lipid. Sci. Technol. 121 (2019) 1900092.
[7] H. Lu, J. Yu, L. Wu, et al., J. Chromatogr. B 1027 (2016) 96–102.
[8] G.F. Xia, X.Y. Fang, Y.R. Wang, X.Y. Yang, Anal. Lett. 50 (2017) 787–796.
[9] M.K. Rai, J.V. Das, V.K. Gupta, Talanta 45 (1997) 343–348.
[10] B. Zhao, Q. Yang, J.S. Wang, et al., New J. Chem. 45 (2021) 4401–4407.
[11] A.P. Vu, T.N. Nguyen, T.T. Do, et al., J. Chromatogr. B 1060 (2017) 111–117.
[12] S. Ali, M.R. Shah, S. Hussain, et al., J. Clust. Sci. 33 (2021) 413–420.
[13] H. Karimi-Maleh, M.L. Yola, N. Atar, et al., J. Colloid Interface Sci. 592 (2021) 174–185.
[14] C. Karaman, O. Karaman, B.B. Yola, et al., New J. Chem. 45 (2021) 11222–11233.
[15] J. Su, S. Zhang, Q. Liu, G. Hu, L. Zhang, J. Mater. Chem. A 9 (2021) 5276–5295.
[16] X. Zhao, X. Li, Z. Bi, et al., J. Energy Chem. 66 (2022) 514–524.
[17] P. Ding, J. Niu, F. Chang, et al., Chin. Chem. Lett. 32 (2021) 2495–2498.
[18] F.Y. Kong, R.F. Li, L. Yao, et al., Nanotechnology 30 (2019) 285502.
[19] X. Shan, J. de Dieu Habimana, J. Ji, et al., J. Solid State Electr. 23 (2019) 1211–1220.
[20] S. Thomas, M. Asle Zaeem, Phys. Chem. Chem. Phys. 22 (2020) 22066–22077.
[21] J. Yu, C. He, C. Pu, et al., Chin. Chem. Lett. 32 (2021) 3149–3154.
[22] J. Jiang, P. Nie, S. Fang, et al., Chin. Chem. Lett. 29 (2018) 624–628.
[23] H. Chakraborty, S. Mogurampelly, V.K. Yadav, U.V. Waghmare, M.L. Klein, Nanoscale 10 (2018) 22148–22154.
[24] A. Prakash, K.B. Sundaram, Appl. Surf. Sci. 396 (2017) 484–491.
[25] J. Houska, P. Steidl, J. Vlcek, J. Martan, Ceram. Int. 42 (2016) 4361–4369.
[26] X. Zhao, M. Zheng, Z. Zhang, et al., J. Mater. Chem. A 9 (2021) 16427–16435.
[27] X. Zhao, Z. Yang, A.V. Kuklin, et al., ACS Appl. Mater. Interfaces 12 (2020) 31419–31430.
[28] F. Ni, Y. Ma, J. Chen, W. Luo, J. Yang, Chin. Chem. Lett. 32 (2021) 2073–2078.
[29] M. Zheng, T. Yuan, J. Shi, W. Cai, X. Wang, ACS Catal. 9 (2019) 8068–8072.
[30] X. Zhao, C. Xiang, F. Zhang, et al., ACS Appl. Mater. Interfaces 11 (2019) 43214–43222.
[31] Z. Chen, M. Lu, Sens. Actuators B: Chem. 273 (2018) 253–259.
[32] M. Li, X. Peng, X. Liu, et al., RSC Adv. 11 (2021) 28988–28995.
[33] Y. Zhu, X. Wang, P. Wang, et al., Ecotox. Environ. Saf. 225 (2021) 112745.
[34] F. Ma, M. Wang, Y. Shao, et al., J. Mater. Chem. C 5 (2017) 2559–2565.
[35] A.A. Moya, J. Phys. Chem. C 120 (2016) 6543–6552.
[36] L.J. Chang, S.H. Luo, H.L. Zhang, et al., Chin. Chem. Lett. 25 (2014) 1569–1572.
[37] K. Ariyoshi, M. Tanimoto, Y. Yamada, Electrochim. Acta 364 (2020) 137292.
[38] H. Huang, L. Kong, W. Shuang, et al., Chin. Chem. Lett. 33 (2021) 1037–1041.
[39] M.S. Pontes, D.R. Antunes, I.P. Oliveira, et al., Environ. Sci. Nano 8 (2021) 1336–1351.
[40] S. Vinoth, P.Mary Rajaitha, A. Pandikumar, Compos. Sci. Technol. 195 (2020) 108192.
[41] T. Morooka, H. Tahara, T. Sagara, Electrochim. Acta 251 (2017) 355–362.
[42] J. Tashkhourian, M. Daneshi, F. Nami-Ana, M. Behbahani, A. Bagheri, J. Hazard. Mater. 318 (2016) 117–124.
[43] H. Hou, B. Wang, Int. J. Quantum Chem. 121 (2021) e26757.
[44] P.Y. Tang, L.J. Han, F.S. Hegner, et al., Adv. Energy Mater. 9 (2019) 1901836.
[45] J. Fangmeyer, A. Behrens, B. Gleede, S.R. Waldvogel, U. Karst, Angew. Chem. Int. Ed. 59 (2020) 20428–20433.
[46] J. Zhang, Z. Lin, Y. Qin, et al., ACS Omega 4 (2019) 18398–18404.
[47] T. Nasir, G. Herzog, M. Hébrant, et al., ACS Sens. 3 (2018) 484–493.
[48] P.B. Deroco, D. Wachholz Junior, L.T. Kubota, Chemosensors 9 (2021) 61.
[49] M. Ghalkhani, S. Maghsoudi, R. Saeedi, S.S. Khaloo, J. Iran. Chem. Soc. 16 (2019) 1301–1309.
[50] L.C.S. de Figueiredo-Filho, M. Baccarin, B.C. Janegitz, O. Fatibello-Filho, Sens. Actuators B: Chem. 240 (2017) 749–756.
[51] J. Li, W. Lei, Y. Xu, et al., Electrochim. Acta 174 (2015) 464–471.
[52] M.A. El Mhammedi, M. Bakasse, A. Chtaini, Electroanalysis 19 (2007) 1727–1733.
[53] K. Charoenkitamorn, C. Chotsuwan, S. Chaiyo, W. Siangproh, O. Chailapakul, Sens. Actuat. B: Chem. 315 (2020) 128089.